Journal of Organometallic Chemistry 868 (2018) 131–143

Contents lists available at ScienceDirect

Journal of Organometallic Chemistry

journal homepage: www.elsevier.com/locate/jorganchem

New ferrocenyl naphthoquinone fused crown ether chemosensors: Highly selective, kinetically and regio controlled colorimetric, beryllium ion recognition

Yusuf Alcay [a], Ozgur Yavuz [a], Ali Gelir [b], Secil Kirlangıc Atasen [a], Kaan Karaoglu [c], Baris Yucel [a], Nurcan Şenyurt Tuzun [a], Ismail Yilmaz [a, *]

[a] Istanbul Technical University, Department of Chemistry, 34469, Maslak, Istanbul, Turkey
[b] Istanbul Technical University, Department of Engineering Physics, 34469, Maslak, Istanbul, Turkey
[c] Recep Tayyip Erdogan University, Vocational School of Technical Sciences, Department of Chemistry and Chemical Process Technology, 53100 Rize, Turkey

ARTICLE INFO

Article history:
Received 11 January 2018
Received in revised form
2 May 2018
Accepted 4 May 2018
Available online 17 May 2018

Keywords:
Ferrocene
Sensor
Beryllium
Naphthoquinone
Colorimetry

ABSTRACT

New organometallic chemosensors which are based on triad molecules, ferrocenyl naphthoquinone linearly/angularly fused crown ethers (**Fc–cnq–1a** and **Fc–cnq–1b)** bearing ferrocene, quinone, and crown ether functional groups together, were synthesized and utilized for selective sensing trace amount of Be^{2+} ion (5.41 μM) among other metal cations. The UV–vis spectrophotometric titration experiments at controlled temperatures (25–60 °C) resulted in characteristic spectral changes in the intramolecular charge-transfer (CT) transitions upon addition of Be^{2+} ion into the solution of sensors **Fc–cnq–1a** and **Fc–cnq–1b**. However, no spectral changes were observed for the other metal cations used for testing at the same conditions, indicating that the sensors can selectively detect Be^{2+} among the studied metal ions even at higher temperatures. The spectral change in the absorption spectra of the sensors upon addition of Be^{2+} ion corresponds to the visible region of the spectrum, from deep green to yellow color, and this leads to observe the effect of the Be^{2+} ion with naked eye. The sensors used for the signaling of Be^{2+} ion displayed a significant shortening in response time depending on increasing temperature without any degradation of the sensors. **Fc–cnq–1a** displayed faster response time than **Fc–cnq–1b** in the temperature range of 35–60 °C. The activation energies for the pseudo-first order complexation reactions were calculated as 124.2±13.0 kJ mol^{-1} and 151.9±18.0 kJ mol^{-1} for **Fc–cnq–1a** and **Fc–cnq–1b**, respectively, which explains faster response time of **Fc–cnq–1a** for recognizing Be^{2+} ion. Density Functional Theory calculations (TD-B97D/TZVP//mPWPW91/6-31 + G(2d,2p) level) were performed on **Fc–cnq–1a**, **Fc–cnq–1b** and their Be^{+2} complexes in order to elucidate their geometries and the molecular orbitals. Calculations have shown comparable results with those obtained from the experimental data.

© 2018 Elsevier B.V. All rights reserved.

1. Introduction

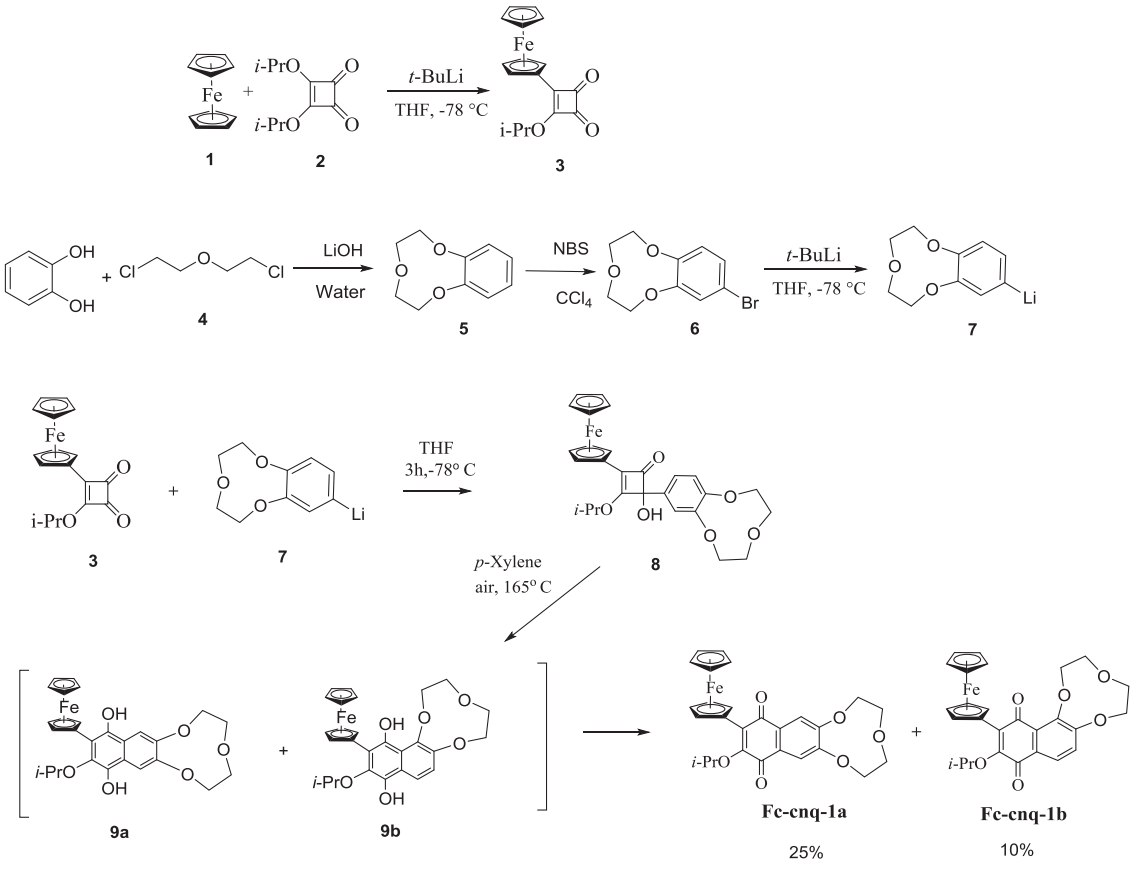
The need for selective and sensitive sensors able to monitor in real-time and real-space the concentration of analytes of biological, clinical, and waste management applications is nowadays generally accepted. Artificial sensors used in these applications can show chromogenic, fluorogenic, and electrochemical selective recognition for a specific molecule or ion [1–14]. On the other hand, Be^{2+} ion recognition studies are little-known among alkali and alkaline earth metals. Although beryllium is the second lightest metal after lithium it is durable metal with many industrial and defense materials applications, including in aerospace, nuclear energy and weapons, electronics and communications, and automobile manufacturing. Additionally, beryllium can be easily alloyed with aluminum, copper or other metals to produce high-performance materials with a variety of attributes [15–17]. Among beryllium compounds, beryllium oxide is effectively used due to its high thermal conductivity and electrical insulation property [18]. These properties allow heat transfer intensely in microscale integrated circuits. Within this wide use framework, beryllium that

* Corresponding author. Istanbul Technical University, Department of Chemistry, 34469, Maslak, Istanbul, Turkey.
E-mail address: iyilmaz@itu.edu.tr (I. Yilmaz).

https://doi.org/10.1016/j.jorganchem.2018.05.004
0022-328X/© 2018 Elsevier B.V. All rights reserved.

contaminates to individuals working in and around the beryllium processing site by inhalation and/or skin contact can cause an immune system failure known as beryllium sensitization, and can lead to documented illnesses of chronic beryllium disease (CBD) or berylliosis, an incurable and potentially fatal progressive lung ailment. The nature and the effects of CBD have been well-studied, but the role of beryllium in triggering CBD is not well understood. The onset of CBD can be delayed for 10–40 years after exposure, and there is no clear dose response correlation. Despite intensive studies on the treatment of the disease, no cures have also been found for CBD or berylliosis until now [19–23]. Hence, beryllium is classified in Group B2 by United States Environmental Protection Agency (USEPA) [24]. International Agency for Research on Cancer (IARC) and World Health Organization (WHO) have highlighted the carcinogenic risks of beryllium and beryllium compounds for humans [25,26]. In spite of the scarcity of beryllium in the earth's crust (2.8–5.0 $\mu g\, g^{-1}$), water supplies and atmosphere are contaminated by beryllium via discharges from anthropogenic sources. Therefore, it is necessary to develop a safe, selective and sensitive techniques for the rapid measurement of beryllium. Some analytical techniques have been used for the determination of the beryllium ion in different samples, e.g. spectrophotometry [27–29], gravimetry [30], chromatography [31–33], spectrofluorimetry [34], gas chromatography [35], atomic absorption spectrometry (AAS) [36], inductively coupled plasma mass spectrometry (ICP-MS) [37]. However, most of these methods are time consuming, relatively expensive, sophisticated, and difficult to operate. This encouraged us to develop new and simply applicable chromogenic chemosensors for detection of Be^{2+} ion. Crown ethers, quinones, and ferrocenes separately or their dyads, have been extensively studied in many applications such as chemical, environmental, clinical, biological, and particularly in material science as well as sensor applications because of their well-known unique properties such as thermal and chemical stability, remarkable metal/molecular binding properties, electron donor/acceptor nature, and electron/proton transfer processes with tunable redox potential [37–53]. However, these unique properties have not been combined on a single molecule, ferrocene-quinone-crown ether molecular triad as chemosensor yet, although ferrocene-quinone [54–56], ferrocene-crown ether [53,57–61] or quinone-crown ether [62–66] molecular dyads have been reported to fulfill varying applications.

In this study, therefore, we have for the first time designed and synthesized new ferrocene-quinone-crown ether triad molecules **Fc–cnq–1a** and **Fc–cnq–1b** as chromogenic organometallic probes for selective sensing trace amount of Be^{2+} ion among Li^{+}, Na^{+}, K^{+}, Cs^{+}, Mg^{2+}, Ca^{2+}, Ba^{2+}, Fe^{2+}, Ni^{2+}, Zn^{2+}, and Pb^{2+} cations. Sensors **Fc–cnq–1a** and **Fc–cnq–1b** were constructed using a regiospecific method involving thermal rearrangement of the reactive ferrocenyl-substituted 4-hydroxy-4-(benzoyl-9-crown-3) cyclobutenone **8** to intermediate hydroquinones **9a and 9b** and its following *in situ* oxidation under air atmosphere (Scheme 1). The strategy employed in the design of these sensors is as follows: first, we introduced a convenient crown ether receptor (benzo-9-crown-3) having a right size (about 0.26 Å) on naphthoquinone core as chelating site for selective binding Be^{2+} ion over other metal ions, where the binding process occurs on the ion-dipole interactions between the macrocyclic ring and Be^{2+} ion. Second, acceptor naphthoquinone core structure was modified by well-known donor ferrocene unit to achieve chromogenic and "naked-eye" recognitions for Be^{2+} ion. The sensors show colorimetric and "naked eye"



Scheme 1. Synthesis of multichannel chemosensors **Fc–cnq–1a** and **Fc–cnq–1b**.

recognition for Be^{2+} ion, which could be monitored by gradually diminishing the intramolecular charge-transfer (ICT) transition between the ferrocenyl donor and naphthoquinonyl acceptor center [e_{π} (HOMO–Fc) → e_{π^*} (LUMO–cnq)] in DMF. In addition to the experiments, the electro-optical properties of **Fc–cnq–1a**, **Fc–cnq–1b** and their Be^{+2} complexes have also been calculated by quantum mechanical calculations in order to elucidate their geometries and the molecular orbitals. Finally, the advantages of selection of organometallic ferrocene–quinone–crown ether as the chemosensors: (1) the selectivity of the sensors is very high, and can selectively detect the Be^{+2} ion among the other metal ions without interference by using spectrophotometric titration technique, (2) the sensors show colorimetric and "naked eye" recognition of Be^{2+} ion, which could be practically monitored by gradually diminishing the intramolecular charge-transfer transition, (3) the response time of the sensors could be controlled depending on the temperature and group position, which is significantly short for practical applications.

2. Experimental section

2.1. General considerations

All chemicals were used as purchased from commercial suppliers without further purification unless otherwise indicated. Diethyl ether and THF (tetrahydrofuran) were freshly distilled from sodium/benzophenone ketyl. Solvents for column chromatography, ethyl acetate and hexane, were distilled in a rotary evaporator. Chromatographic separations were performed with Merck Silica 60 (200–400 or 70–230 mesh). TLC (Thin-Layer Chromatography) was performed with Merck TLC Silicagel 60 F254 plates, detection was carried out under UV light at 254 nm.

The compounds **2**, **3** [67], **4** and **5** [68] given in Scheme 1 were prepared according to known literature methods.

2.2. Measurements

NMR spectra were recorded with an Agilent VNMRS 500 (500 MHz for ^{1}H and 125 MHz for ^{13}C NMR) instrument. Chemical shifts δ were given in ppm relative to residual peaks of deuterated solvents and coupling constants, J, were given in Hertz. The following abbreviations are used to describe spin multiplicities in ^{1}H NMR spectra: s = singlet; d = doublet; t = triplet; q = quartet; dd = doublet of doublets; m = multiplets. IR spectra were recorded on Perkin–Elmer FT–IR spectrometer. Low resolution mass spectra (API-ES, 70 eV, and APCI) were obtained on an Agilent 1100 GC-MS instrument equipped with a diode array UV–Visible (UV–vis) range detector and Thermo LCQ Deca Ion Trap Mass Spectrometer (Thermo Finnigan). High resolution mass spectra (HRMS) were obtained on a Waters Synapt Q-TOF-MS spectrometer. Elemental analysis was carried out by the CHNS Elemental Analyzer instrument in TÜBİTAK (MAM). UV–vis spectra were recorded on Agillent Model 8453 diode array spectrophotometer. Kinetically controlled selective cation binding studies were performed with UV–vis spectrophotometric titration technique at varying temperatures (25–60 °C). The solutions of 3 mL and 3.0×10^{-4} M **Fc–cnq–1a** and **Fc–cnq–1b**, in DMF were taken into the cell where constant temperatures are regulated by a thermostat. Alkali metals (Li^+, Na^+, K^+ and Cs^+), alkaline earth metals (Mg^{2+}, Ca^{2+} and Ba^{2+}) perchlorates, transition metals (Fe^{2+}, Ni^{2+}, Zn^{2+}) chlorides, Pb^{2+} (as lead acetylacetonate ($Pb(acac)_2$), and $BeCl_2$, were used during the UV–vis or voltammetric measurements. Methodology for the details of Density Functional Theory calculations is given in the Supporting Information.

2.3. Synthesis of 9-bromo-2,3,5,6-tetrahydrobenzo[b][1,4,7] trioxonine (6)

2,3,5,6-tetrahidro-benzo[b][1,4,7]trioxonine **5** (2.00 g, 0.011 mol) and *N*-bromosuccinimide (NBS) (1.98 g, 0.011 mol) were refluxed in carbon tetrachloride (CCl_4) (25 mL) for 2 h. The reaction mixture was cooled to room temperature, and filtered. The filtrate was evaporated to dryness in a rotary evaporator. Oily residue was subjected to the chromatography on silica gel using dichloromethane (CH_2Cl_2) as eluent to yield **6**. Yield: 1.30 g (46%). $R_f = 0.39$ (CH_2Cl_2). ^{1}H NMR (500 MHz, $CDCl_3$): δ = 3.91–3.93 (m, 4 H, 2 × CH_2), 4.32–4.38 (m, 4 H, 2 × CH_2), 6.87–7.15 (m, 3 H, Ar); ^{13}C NMR (125 MHz, $CDCl_3$): δ = 72.34 (CH_2), 72.38 (CH_2), 74.03 (CH_2), 74.16 (CH_2), 115.37 (CH, Ar), 124.39 (CH, Ar), 125.90 (CH, Ar), 126.79 (C_{quat}), 150.72 (C_{quat}), 147.82 (C_{quat}), 152.17 (C_{quat}). IR (ATR): $\tilde{\nu}$ (cm^{-1}) = 3050, 2920, 2861, 1585, 1492, 1450, 1403, 1365, 1301, 1259, 1201, 1127, 1076, 1036, 923, 902, 835, 639. GCMS: *m*/*z* (%): 260.0 (80) $[M+H]^+$. HRMS [TOF MS ES$^+$]: *m*/*z* [M-Br-2H]$^+$ Anal. calcd for ($C_{10}H_9O_3$) 177.0552 g/mol, found, 177.0602 (28.2 ppm).

2.4. Syntheses of 10-isopropoxy-11-ferrocenyl-2,3,5,6-tetrahydronaphtho[2,3-b][1,4,7]trioxonine-9,12-dione(Fc–cnq–1a),11-isopropoxy-12-ferrocenyl-2,3,5,6-tetrahydronaphtho[1,2b][1,4,7]tri-oxonine-10,13-dione (Fc–cnq–1b)

A solution of **6** (1.00 g, 3.85 mmol) in dry THF (25 mL) was cooled to -78 °C under nitrogen atmosphere. To this solution after 5 min, *n*-BuLi (3.33 mL or 1.4 equiv of a 1.6 M of hexane solution) was added via syringe in 15 min. The resulting mixture was stirred at -78 °C for 1 h. A solution of 3-ferrocenyl-4-isopropoxy-3-cyclobutene-1,2-dione **3** (1.25 g, 3.85 mmol) was prepared in dry THF (25 mL) at -18 °C under the nitrogen atmosphere in a different flask and it was slowly transferred via cannula to the mixture containing **7** at -78 °C. This reaction mixture was stirred at -78 °C for 30 min, then it was continued at 0 °C for 2 h. After this reaction period, the reaction mixture was quenched with H_2O, and then allowed to warm to room temperature. The mixture was diluted with ether and the organic layer was separated. The aqueous layer was extracted with ether which was dried over Mg_2SO_4 and filtered. The solution was concentrated in a rotary evaporator and the remaining crude material was dissolved in *p*-xylene. The resulting solution was heated at reflux open to the air in a preheated oil bath (165 °C) for 3 h. After removal of the *p*-xylene in a rotary evaporator, the green solid residue was subjected to the chromatography on silica gel using 2:1 hexane/ethyl acetate as eluent to yield a mixture of the green products (**Fc–cnq–1a** and **Fc–cnq–1b**). These two products were separated by applying a second chromatography on silica gel using CH_2Cl_2 as eluent. For **(Fc–cnq–1a)**, yield: 0.483 g (25%). $R_f = 0.42$ (CH_2Cl_2). ^{1}H NMR (500 MHz, $CDCl_3$): δ = 1.27 (d, *J* = 6.1 Hz, 6 H, 2 × *i*PrO [CH_3]), 3,95 (s, 4 H, 2 × CH_2) 4.12 (s, 5 H, Fc), 4.51 (s, 4 H, 2 × CH_2), 4.55 (s, 2 H, Fc), 4.81–4.86 (m, 1 H, *i*PrO [CH]), 5.18 (s, 2 H, Fc), 7.64 (s, 1 H, Ar), 7.68 (s, 1 H, Ar). ^{13}C NMR (125 MHz, $CDCl_3$): δ = 22.77 (2 × CH_3, *i*PrO), 70.02 (5 × CH, Fc), 70.22 (2 × CH, Fc), 72.33 (CH_2), 72.37(CH_2), 72,79(2 × CH, Fc), 73.36 (CH_2), 73.54 (CH_2), 74.73 (C_{quat}, Fc), 76.21 (CH, *i*PrO), 120.61 (CH, Ar), 121.27 (CH, Ar), 127.75 (C_{quat}), 129.31 (C_{quat}), 136.18 (C_{quat}), 154.79 (C_{quat}), 155.36 (C_{quat}), 155.70 (C_{quat}), 180.04 (C_{quat}; C=O), 183.63 (C_{quat}; C=O). IR (ATR): $\tilde{\nu}$ (cm^{-1}) = 3050, 2919, 2850, 1651, 1590, 1556, 1461, 1383, 1338, 1296, 1179, 1077, 1023, 1000, 900, 803, 744. HRMS [TOF MS ES$^+$]: *m*/*z* $[M+H]^+$ Anal. calcd for ($C_{27}H_{27}FeO_6$) 503.1149 g/mol, found, 503.1129 (−1.6 ppm). For (**Fc–cnq–1b**), yield: 0.193 g (10%) $R_f = 0.32$ (CH_2Cl_2). ^{1}H NMR (500 MHz, $CDCl_3$): δ = 1.28 (d, *J* = 6.4 Hz, 6 H, 2 × *i*PrO [CH_3]), 3.98–4.00 (m, 4H, 2 × CH_2), 4.13 (s, 5 H, Fc), 4.30–4.32 (m, 2H, CH_2),

4.49 (s, 2 H, Fc), 4.65–4.67 (m, 2H, CH_2) 4.87–4.92 (m, 1 H, *i*PrO [CH]), 5.16(s, 2 H, Fc), 7.23 (d, $J = 8.6$ Hz, 1 H, Ar); 7.81 (d, $J = 8.1$ Hz, 1 H, Ar). ^{13}C NMR (125 MHz, $CDCl_3$): $\delta = 22.76$ ($2 \times CH_3$, *i*PrO), 70.00 ($5 \times$ CH, Fc), 70.20 ($2 \times$ CH, Fc), 72.32 (CH_2), 72.37(CH_2), 72,77($2 \times$ CH, Fc), 73.36 (CH_2), 73.53 (CH_2), 74.70 (C_{quat}, Fc), 76.20 (CH, *i*PrO), 120.61 (CH, Ar), 121.27 (CH, Ar), 127.75 (C_{quat}), 129.31 (C_{quat}), 136.16 (C_{quat}), 154.80 (C_{quat}), 155.36 (C_{quat}), 155.70 (C_{quat}), 180.04 (C_{quat}; C=O), 183.63 (C_{quat}; C=O). IR (ATR): $\tilde{\nu}$ (cm^{-1}) = 2982, 2869, 1651, 1590, 1462, 1338, 1296, 1178, 1087, 1023, 1000, 913, 815, 745. HRMS [TOF MS ES$^+$]: *m*/*z* [M+H]$^+$ Anal. calcd for ($C_{27}H_{27}FeO_6$) 503.1157 g/mol, found, 503.1155(−0.4 ppm).

3. Result and discussion

3.1. Syntheses of new probes (*Fc–cnq–1a* and *Fc–cnq–1b*)

Scheme 1 represents the reaction route for the synthesis of new probes **Fc–cnq–1a** and **Fc–cnq–1b** which were synthesized by the reaction of 3-ferrocenyl-4-isopropoxy-3-cyclobutene-1,2-dione **3** and 9-lithio-2,3,5,6-tetrahydrobenzo[b] [1,4,7]trioxonine **7** according to literature procedure [54,55,67,69]. **3** and **5** compounds are not commercially available so they were also synthesized according to the procedure given in literature [67,68]. Briefly, the starting material ferrocenyl cyclobutenedione **3** was synthesized by the reaction of diisopropyl squarate **2** and ferrocenyl lithium prepared *in-situ* by the treatment of *t*-BuLi with ferrocene **1** under a nitrogen atmosphere in dry THF.

The solution of ferrocenyl lithium was transferred into diisopropyl squarate **2** in dry THF at −78 °C via a cannula to prevent air contact. After the addition of acetic anhydride to the resulting solution and the stirring of the solution overnight at room temperature, ferrocenyl cyclobutenedione **3** was obtained in 60% yield. The crown ether **5** was synthesized by the reaction of catechol and 1,5-dichloro-3-oxapentane **4**. **7** was prepared from 9-bromo-2,3,5,6-tetrahydrobenzo[b] [1,4,7]trioxonine **6** and *n*-butyllithium (*n*-BuLi) as a mixture in THF at −78 °C under a nitrogen atmosphere for 1 h. Solution of **3** in a different reaction vessel at low temperature (−18 °C) under the nitrogen atmosphere was slowly transferred by means of a cannula into **7**. **Fc–cnq–1a** and **Fc–cnq–1b** were obtained without isolation and purification of ferrocenyl-substituted 4-hydroxy-4-(benzoyl-9-crown-3)cyclobutenone **8**. This crude product was dissolved in *p*-xylene and refluxed open to air to accelerate oxidation of the intermediate hydroquinones **9a** and **9b**. The reaction progress was easily monitored by TLC and observed the change in color of the solution from deep purple to deep green. Finally, crude products were collected as an isomeric mixture (**Fc–cnq–1a** and **Fc–cnq–1b**) after evaporation of the solvent under vacuum. These isomers were successfully separated by the sequential two column chromatography on silica gel. By this way, **Fc–cnq–1a** and **Fc–cnq–1b** were obtained with 25% and 10% yields, respectively. In this procedure, **Fc–cnq–1a** and **Fc–cnq–1b** were obtained in a shorter time, in a higher yield, and consumed less chemicals such as solvents and silica gel without the isolation of the 4-hydroxycyclobutenone derivative **8** as we know that the column chromatography is considerably tedious, and 4-hydroxycyclobutenone derivatives may rapidly decompose even if they are kept under the nitrogen atmosphere at room temperature. Similar to our previous report [69], water was used as a quencher instead of NH_4Cl solution due to binding NH_4^+ cation with crown ether macrocyclic, leading to eliminate quencher effect. It is well-known that the thermal rearrangements of 4-aryl-4-hydroxycyclobutenones may yield two regioisomeric naphthoquinones via ring closure at two different positions of aryl groups (α or β positions) [54]. Therefore, the thermolysis of the cyclobutenone **8** yielded the linearly and angularly-fused naphthoquinone **Fc–cnq–1a** and **Fc–cnq–1b** (Scheme 1). Finally, **6**, new probes **Fc–cnq–1a** and **Fc–cnq–1b** were elucidated by various techniques such as Elemental Analysis, FTIR, ^{1}H and ^{13}C NMR, HRMS and UV–vis as shown in Figs. S1- S11 and Fig. 1.

3.2. Selectively and kinetically controlled colorimetric sensing Be^{2+} ion

UV–vis absorption spectra of **Fc–cnq–1a** (black line) and **Fc–cnq–1b** (red line) in the 200–1100 nm range in DMF solution are shown in Fig. 1. As seen from the general view of the spectra, electronic behaviors of probes **Fc–cnq–1a** and **Fc–cnq–1b** are quite similar to each other, and to what we observed for the ferrocenyl naphthoquinones reported in our previous work [54,55,69], only with a difference in their peak positions due to attachment of different groups to naphthoquinone core. It can be expressed in a general approach that the spectra of **Fc–cnq–1a** and **Fc–cnq–1b** display strong intensity bands at 292 nm and 284 nm with two moderate intensity bands at 333 nm and 425 nm, 354 nm and 425 nm, respectively, which are characteristic transitions (n, π → π*) of naphthoquinone.

Fc–cnq–1a and **Fc–cnq–1b** also exhibit distinctive bands at 670 nm and 649 nm, respectively, which are assigned to the intramolecular charge-transfer (CT) transitions basically taking place between the ferrocenyl donor and the naphthoquinonyl acceptor center [eπ (HOMO–ferrocene) → eπ* (LUMO–naphthoquinone)]. These main transitions lead to green color of **Fc–cnq–1a** and **Fc–cnq–1b**, and similar to the previously well-characterized the CT transitions of ferrocene–DDQ (2,3-dichloro-5,6-dicyanobenzoquinone) [e_π (HOMO–Fc) → e_{π^*} (LUMO–DDQ)] and ferrocene–benzoquinone [e_π (HOMO–Fc) → e_{π^*} (LUMO–q) donor-acceptor dyads [54,69–73]. When compared with **Fc–cnq–1a** and **Fc–cnq–1b**, the CT bands for **Fc–cnq–1a** is red-shifted by 21 nm. We evidently know from our previous work that the electron-donating or electron-withdrawing substituents with their positions attached to ferrocenyl-naphthoquinones shifts the CT bands to higher energy or lower energy, respectively, compared to parent ferrocenyl-naphthoquinone without substituent [54,69]. Therefore, it is obvious that this observation arises from the weaker electron-donating ability of the crown ether groups linearly fused to the naphthoquinone core than the groups angularly fused to the naphthoquinone core. The crown ether group in **Fc–cnq–1a** can serve as a receptor as expected, and the interaction

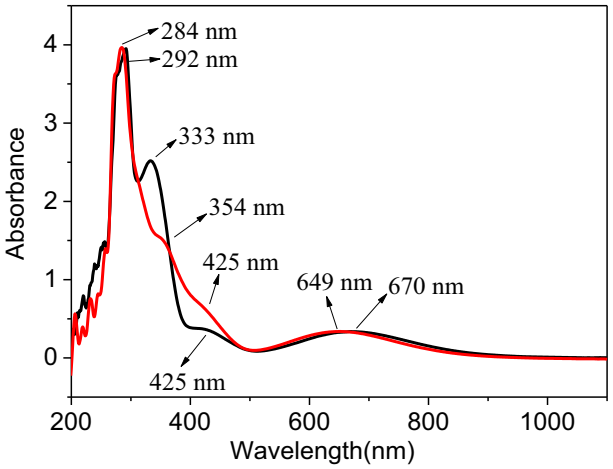


Fig. 1. UV–vis spectra of **Fc–cnq–1a** (black line) and **Fc–cnq–1b** (red line) in DMF ($c = 3.0 \times 10^{-4}$ M). (For interpretation of the references to color in this figure legend, the reader is referred to the Web version of this article.)

between the receptor and particularly Be^{2+} ion, leads to dramatic changes in the absorption spectra of **Fc–cnq–1a** and **Fc–cnq–1b** at 25 ± 0.01 °C in DMF (Fig. 2a and b). It was clearly seen from Fig. 2a that the CT transition band at 670 nm, which monotonically decreased and almost completely disappeared upon saturation of **Fc–cnq–1a** with Be^{2+} ion. Besides, the bands at 292 and 425 nm visibly decreased and the band at 333 nm increased. The spectral changes obtained in this experiment showed a clear isosbestic points at 294 nm, 415 nm, and 516 nm, confirming that the binding reaction between the probe and Be^{2+} ion proceeded in a quantitative fashion to form the complex and the absence of any degradation or side reactions during the complexation based on the ion-dipol interaction between Be^{2+} ion and crown ether unit [54,69,74–78].

In parallel with these explanations, probe **Fc–cnq–1b** also exhibited characteristic spectral changes upon addition Be^{2+} ion into the solution of **Fc–cnq–1b**, which was almost the same as that observed for **Fc–cnq–1a** in the identical condition with an exception of its peak position as expected (Fig. 2b). These distinct changes in the absorptions of probes **Fc–cnq–1a** and **Fc–cnq–1b** participated in the change in color of the solution from deep green to yellow, which enabled us to detect Be^{2+} ion with naked eye. Unlike Be^{2+} ion, when Li^{+}, Na^{+}, K^{+}, Cs^{+}, Mg^{2+}, Ca^{2+}, Ba^{2+}, Fe^{2+}, Ni^{2+}, Zn^{2+}, and Pb^{2+} cations were added into the solution of **Fc–cnq–1a** and **Fc–cnq–1b** in the same experimental condition, it was seen that these metal ions did not affect the absorption spectra of **Fc–cnq–1a** and **Fc–cnq–1b** (Fig. 3a and b). These results evidently confirm that **Fc–cnq–1a** and **Fc–cnq–1b** can specifically signal Be^{2+} even in the presence of such metal cations with high concentrations (Fig. S12). On the other hand, to determine response time of the sensors, we presented the plots of absorbance versus time as insets in Fig. 2, where the absorbances were recorded for the CT transitions at 670 nm for **Fc–cnq–1a** and that at 649 nm for **Fc–cnq–1b** in the presence of Be^{2+} ion. It revealed that the response times for the probes **Fc–cnq–1a** and **Fc–cnq–1b** were 250 min and 230 min, respectively at 25 ± 0.01 °C in DMF, which were fairly high period of time, and reduced practical applicability of the sensors. Therefore, the probes **Fc–cnq–1a** and **Fc–cnq–1b** were investigated at controlled temperatures (25–60 °C) in DMF, maintaining their stable form, to find out both their selective sensing behavior of Be^{2+} ion over the studied metal ions and particularly reasonable response times. For this purpose, the absorption spectra **Fc–cnq–1a** and **Fc–cnq–1b** were taken separately at different temperatures (in the range of 25–60 °C) in the presence of Be^{2+} and the tested metal cations in DMF.

The corresponding absorption spectra of **Fc–cnq–1a** and **Fc–cnq–1b** in the presence of Be^{+2} ion are given in Fig. 4 and in the presence of other metal ions are presented in Figs. S13–S18. As can

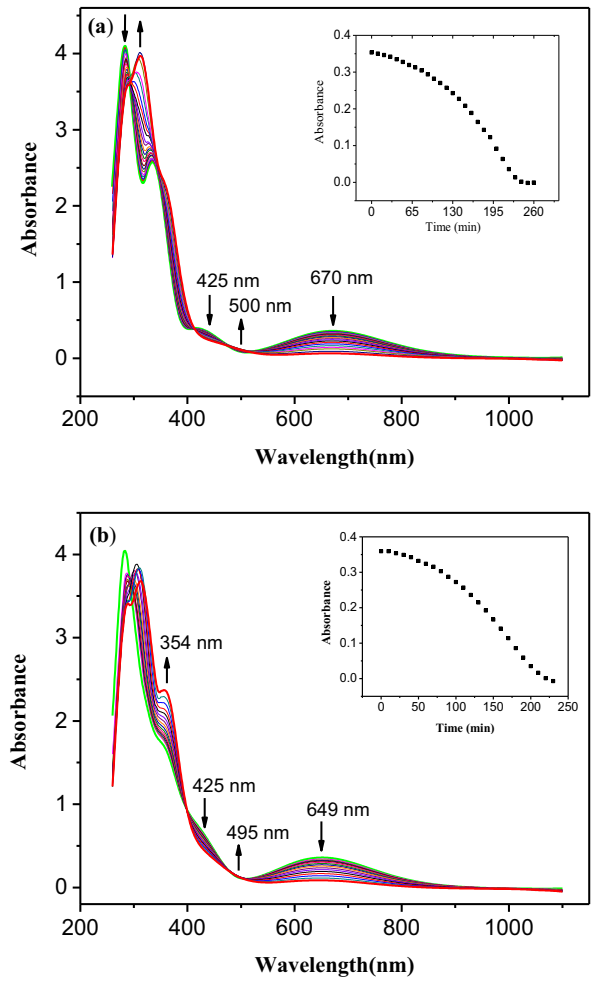


Fig. 2. UV–vis spectral changes of **Fc–cnq–1a** (a) and **Fc–cnq–1b** (b) upon addition of Be^{2+} at 25 ± 0.01 °C in DMF (5.0×10^{-2} M). Inset: plot of absorbance *vs* time. Concentration of **Fc–cnq–1a** and **Fc–cnq–1b** is 3.0×10^{-4} M.

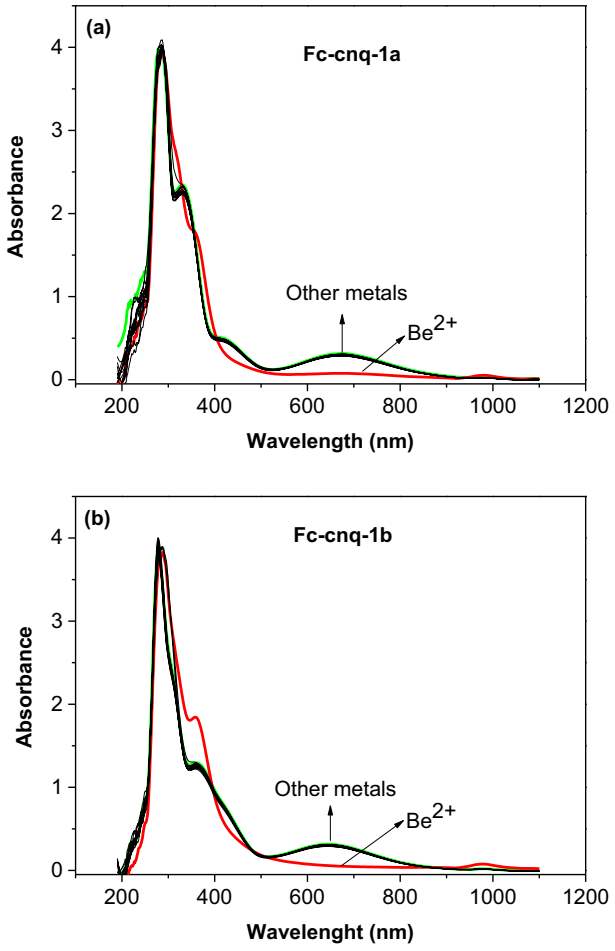


Fig. 3. Absorption spectra of **Fc–cnq–1a** (a) and **Fc–cnq–1b** (b) at 25 °C ± 0.01 in DMF after the addition of different metal ions. Other metals: Li^{+}, Na^{+}, K^{+}, Cs^{+}, Mg^{2+}, Ca^{2+}, Ba^{2+}, Fe^{2+}, Ni^{2+}, Zn^{2+}, and Pb^{2+} (5.0 equiv). Red solid line represents Be^{2+} ion (1.0 equiv). Concentration of **Fc–cnq–1a** and **Fc–cnq–1b** = 3.0×10^{-4} M. (For interpretation of the references to color in this figure legend, the reader is referred to the Web version of this article.)

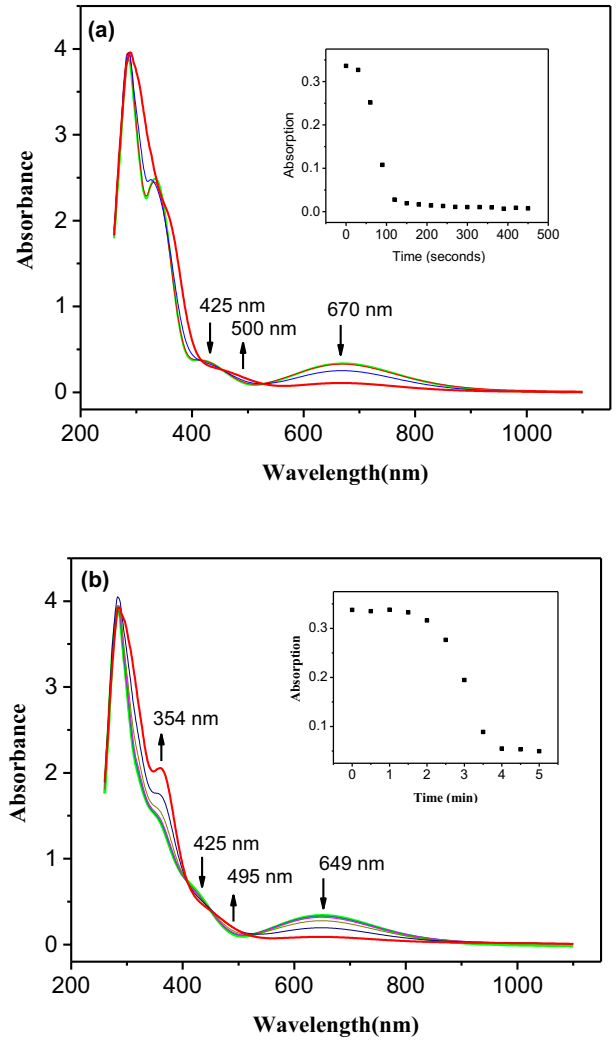


Fig. 4. UV–vis spectral changes of **Fc–cnq–1a** (a) and **Fc–cnq–1b** (b) upon addition of Be^{2+} (5.0×10^{-2} M) at 60 ± 0.01 °C in DMF. Inset: plot of absorbance *vs* time. Concentration of **Fc–cnq–1a** and **Fc–cnq–1b** is 3.0×10^{-4} M.

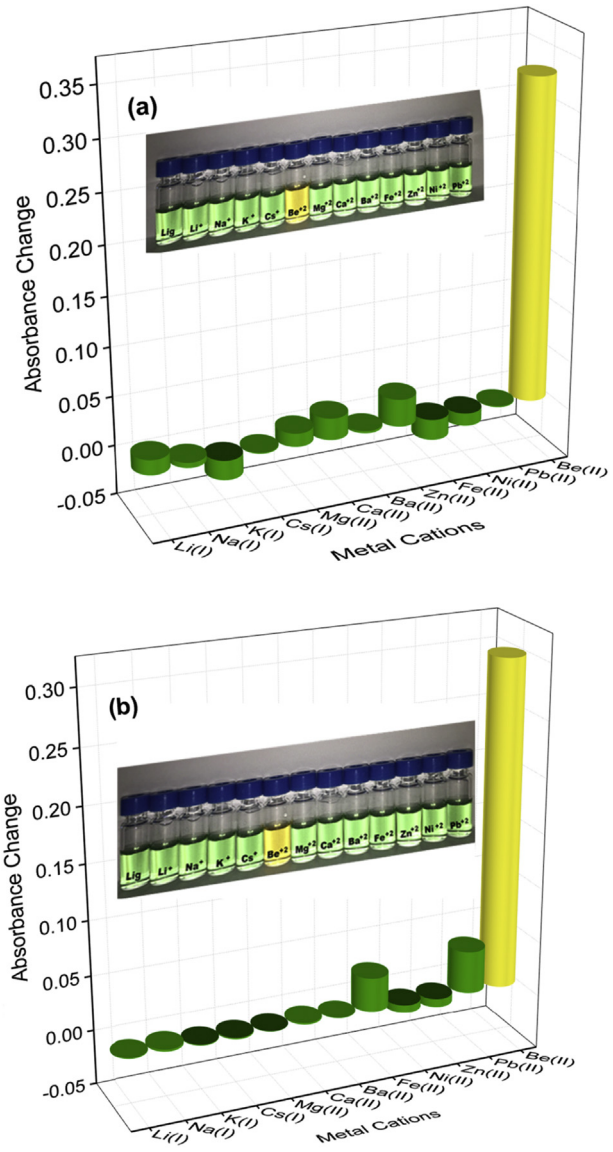


Fig. 5. The absorption changes at 670 nm for **Fc–cnq–1a** (3.0×10^{-4} M) (a), and at 649 nm for **Fc-cnq-1b** (3.0×10^{-4} M) (b) in the presence of Be^{2+} (1.0 equiv) and other metal ions (5.0 equiv) at 60 ± 0.01 °C in DMF. Insets represent visual changes upon addition of various metal ions to the solutions, where Lig represents free sensors **Fc–cnq–1a** and **Fc–cnq–1b**.

be seen clearly from these figures that the spectral changes observed at all studied temperatures in the presence of Be^{2+} are almost similar to those observed at 25 ± 0.01 °C in DMF. Additionally, no spectral changes for **Fc–cnq–1a** and **Fc–cnq–1b** were observed for the tested metal cations at these conditions, indicating that the sensors **Fc–cnq–1a** and **Fc–cnq–1b** can selectively detect Be^{2+} among the studied metal ions even at higher temperatures (Fig. 5). The selectivity of Be^{2+} ion over the studied metals was obviously detected by naked eye as seen from insets in Fig. 5 where the color of the solution changed to yellow upon interacting the sensors with the Be^{+2} ion while no change in the color of the solutions was observed for the other metal cations.

The time behaviors of the complexation reaction between probes **Fc–cnq–1a** and **Fc–cnq–1b**, and Be^{+2} ion at different temperatures were represented in Fig. 6. Here, it was seen that at temperatures below 40 °C, a delay at the beginning of the reaction was observed. At higher temperatures, almost no delay was observed and the complexation reaction started immediately. The delay at the beginning may correspond to the time for the homogeneous distribution of Be^{2+} ions around the sensors. At low temperatures, this takes much longer time and at higher temperatures the cations can be reorganized around the receptors in shorter times due to their higher kinetical energy.

Fig. 7 shows response time versus temperature for **Fc–cnq–1a** and **Fc–cnq–1b** at different temperatures. Therein, the response times were recorded when the CT transition bands at 670 nm for **Fc–cnq–1a** and that at 649 nm for **Fc–cnq–1b** were reached almost zero in the presence of Be^{2+} ion at elevating temperatures. As seen that the response time is considerably affected by the reaction temperature.

According to the Arrhenius theorem [79], we expect chemical reactions to go faster at higher temperatures, and thus the complexation reaction between the sensors and Be^{2+} ion took place in a shorter times as it was observed in Figs. 6 and 7 where the response times have dropped to 2 min and 4 min at 60 °C for the sensors **Fcnq–1a** and **Fc–cnq–1b**, respectively, without any degradation of the sensors. However, at lower temperatures, below 45 °C, some fluctuations between probes **Fc–cnq–1a** and

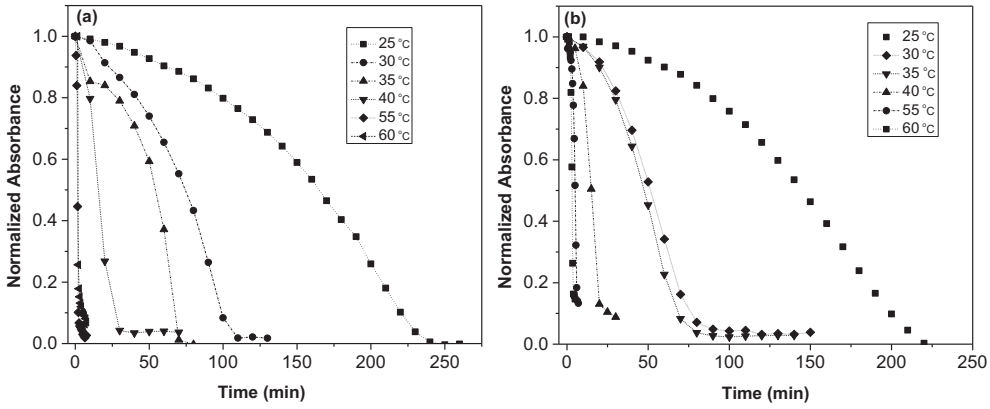


Fig. 6. Normalized absorbance *vs* time plots for probes **Fc–cnq–1a** (a) and **Fc–cnq–1b** (b) at different temperatures. [**Fc–cnq–1a]** and **[Fc–cnq–1b]** = 3.0×10^{-4} M **[Be**$^{2+}$**]** = 5.4×10^{-2} M.

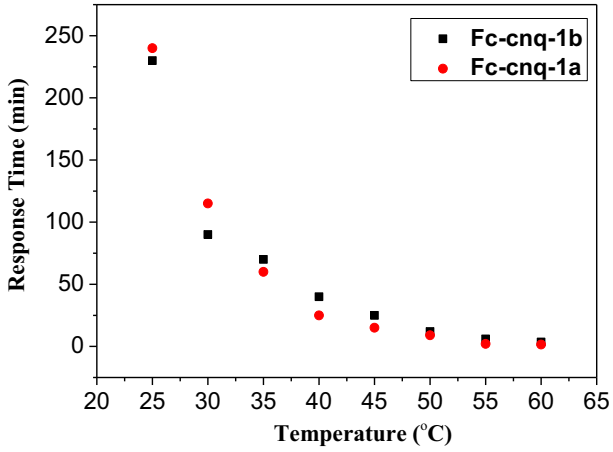


Fig. 7. Response time *vs* temperature plots for probes **Fc–cnq–1a** (a) and **Fc-cnq-1b** (b).

Fc–cnq–1b were observed, but when the temperature was increased, the behavior of the ligands almost the same with each other. When compared **Fc–cnq–1a** with **Fc–cnq–1b** in terms of their response times, **Fc–cnq–1a** responses faster than **Fc–cnq–1b** at 35–60 °C, which is probably due to having lower activation energy of **Fc–cnq–1a** confirmed by the kinetic study reported below. In order to clarify the stability of the probes, the absorption spectra **Fc–cnq–1a** and **Fc–cnq–1b** were successively taken at 60 °C, the maximum working temperature, in the absence of Be^{2+} ion for a long period of time, and no change in absorbance or peak position of the maximum absorbance were observed, indicating that **Fc–cnq–1a** and **Fc–cnq–1b** do not undergo decomposition or photobleaching during the measurement time (black squares in Fig. 8). However, when Be^{+2} ion is added to the solution, complexation reaction occurs between the sensor and Be^{+2} ion and the absorbance goes to almost zero in shorter times (red circles in Fig. 8) due to the reasons mentioned in above paragraphs.

The results of the fitting of the experimental data obtained from the reaction of **Fc–cnq–1a** with Be^{+2} ion at 40 °C to the pseudo-first order and pseudo-second order reaction laws were represented in Fig. 9. This data was given as an example and the same procedure was applied to the measurements performed at the other temperatures to determine the reaction order. It is clearly seen from Fig. 9 that, the R-square value obtained from the pseudo-first order fitting in Figure 9a and 0.9907, is higher than that was obtained from the pseudo-second order fitting in Fig. 9b and 0.5794. According to this result it is assumed that the order of the reaction is pseudo-first order [79].

The activation energy of the reaction was calculated according to the Arrhenius equation given as,

$$k(T) = k_0 e^{-\Delta E/RT} \quad (1)$$

where k is the rate constant, ΔE is the activation energy, R is universal gas constant and T is the temperature.

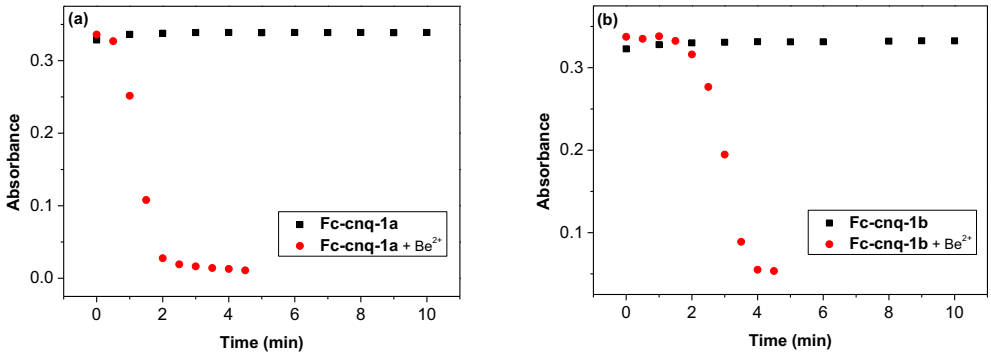


Fig. 8. The plots of absorbance *vs* time for **Fc–cnq–1a** (a) and **Fc–cnq–1b** (b) in the absence of Be^{2+} ion (black squares), and in the presence of excess amount of Be^{2+} ion (red circles) at 60 ± 0.01 °C in DMF. Concentration of **Fc–cnq–1a** and **Fc–cnq–1b** = 3.0×10^{-4} M. (For interpretation of the references to color in this figure legend, the reader is referred to the Web version of this article.)

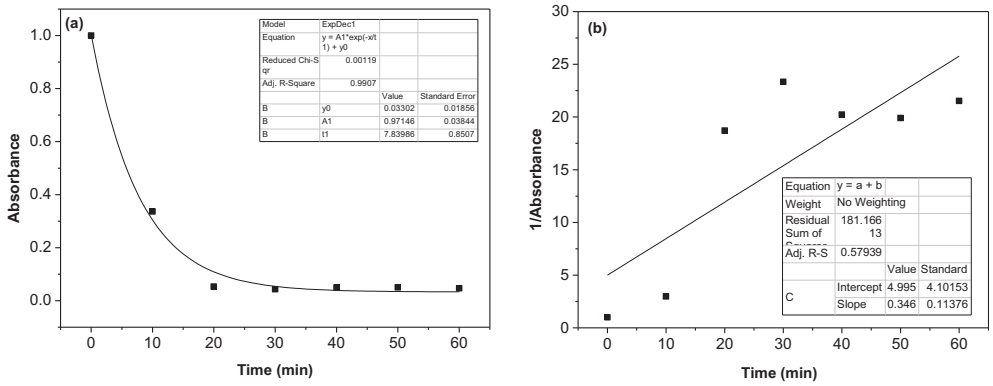


Fig. 9. Comparison of the pseudo-first order (a) and pseudo-second order (b) reaction equations for the experimental data obtained from the reaction of the sensor **Fc–cnq–1a** with Be^{+2} ion at 40 °C.

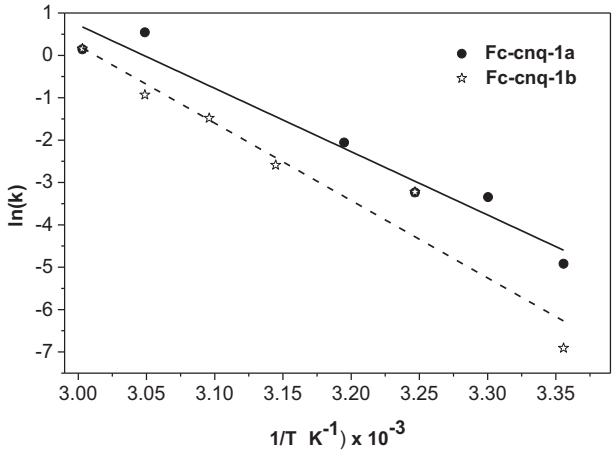


Fig. 10. Arrhenius plots of the complexation reactions of **Fc–cnq–1a**/Be^{+2} and **Fc-cnq–1b**/Be^{+2} systems.

The variation of the natural logarithms of the rate constants obtained at different temperatures for the ligands **Fc-cnq-1a** and **Fc-cnq-1b** were plotted against 1/T in Fig. 10. By fitting these experimentally obtained rate constants to the natural logarithm of Eq. (1), the activation energies of the complexation reactions between the sensors and the Be^{+2} were calculated as 124.2±13.0 kJ mol^{-1} and 151.9±18.0 kJ mol^{-1} for the sensors **Fc–cnq–1a** and **Fc–cnq–1b**, respectively, which could clearly explain why **Fc–cnq–1a** displayed shorter response time than that of **Fc–cnq–1b** for recognizing Be^{2+} ion.

In the light of these studies, UV–vis spectrophotometric titration method was carried out by using probes **Fc–cnq–1a** and **Fc–cnq–1b** for quantitative determination of Be^{2+} ion at 60 °C as the optimum temperature in DMF (Fig. 11). The insets in Fig. 11 show the plot of absorbance versus the ratio of concentrations of the sensors and Be^{+2} ion where the absorbances were recorded at 670 nm for **Fc–cnq–1a** and at 649 nm for **Fc–cnq–1b** in the presence of Be^{2+}. Job's plot analysis for both **Fc-cnq-1a/1b** towards Be^{2+} ion was performed to examine the stoichiometry of the binding. In Fig. S19, the absorptions at 670 nm and 649 nm are plotted against molar fraction of chemosensors, **Fc–cnq–1a** and **Fc–cnq–1b** under a constant total concentration. Maximum intensity was reached when the molar fraction was 0.5. These results indicate a 1:1 binding stoichiometry.

The 1:1 complexation of metal cation, Be^{2+}, with sensors, **Fc–cnq–1a** and **Fc–cnq–1b**, is given by the following equilibrium equation:

$$M + L \xrightarrow{K} ML \tag{2}$$

where K is the binding constant and is defined as

$$K = \frac{[M][L]}{[ML]} \tag{3}$$

where [M], [L] and [ML] are the concentrations of the free cation, free sensor and complex molecules, respectively.

Benesi-Hildebrand method, which is suitable for the calculation of the binding constant of complexes with 1:1 binding ratio, was used to calculate K [80–83]. The expression of the Benesi-Hildebrand method in terms of the absorption is given by

$$\frac{1}{\Delta A} = \frac{1}{(A_{max} - A)Kc_M} + \frac{1}{(A_{max} - A)} \tag{4}$$

where $\Delta A = A_o - A$, A_o and A are the absorbances of the sensors in the absence and presence of the cation, respectively, A_{max} is the absorbance of the ligand when the maximum amount of the cation was added, K is the binding constant and c_M is the concentration of the metal cation.

Benesi-Hildebrand plots of the ligands **Fc–cnq–1a** and **Fc–cnq–1b** were represented in Fig. 12. A good linear behavior was observed for each complex. The binding constant of the complexation reactions of **Fc-cnq-1a** and **Fc-cnq-1b** were calculated by dividing the intercept with the slope according to Eq. (4) and found to be 591.5±23.3 M^{-1} and 1116.7±11.7 M^{-1}, respectively. Also, the standard Gibbs free energy change for these complexation reactions were also calculated as −17.7±0.1 and −19.4±0.2 kJ mol^{-1} for the ligands **Fc–cnq–1a** and **Fc–cnq–1b**, respectively. These results indicate that **Fc–cnq–1b**, the ferrocenyl naphthoquinone angularly fused crown ether unit, binds Be^{2+} ion more strongly than that of **Fc–cnq–1a**, the ferrocenyl naphthoquinone linearly fused crown ether group.

The detection limits of sensors **Fc–cnq–1a** and **Fc–cnq–1b** for the analysis of Be^{2+} were estimated from the titration results in the range of 8.3 μM–1.1 mM (Fig. 11c and d), and found to be 5.4 μM, which was calculated with the equation of 3σ/S. σ is the standard deviation of the absorption intensity of sensors, S is the slope between the absorption intensity vs concentration. It means that it is able to detect Be^{2+}concentrations in the micro-molar range, and be found in moderately data for spectroftometric Be^{2+} sensors [27–29,34]. However, new organometallic molecules can be promising chemical sensors as highly selective in the presence of

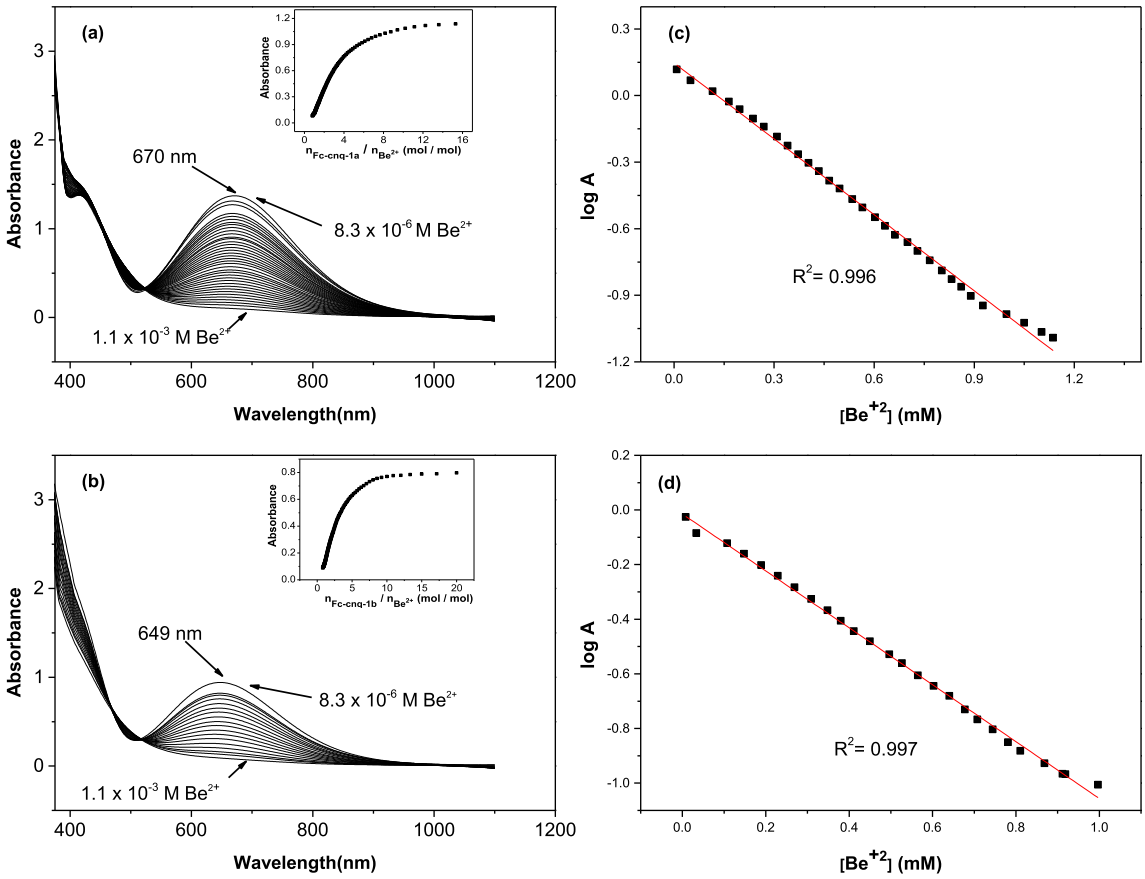


Fig. 11. Absorbance responses of **Fc–cnq–1a** (a) and **Fc–cnq–1b** (b) upon addition of aliquots of $BeCl_2$ at 60 ± 0.01 °C in DMF, insets show a plot of absorbance *vs* n (**Fc–cnq–1a**) or n (**Fc–cnq–1b**)/n^{2+}_{Be} (mol/mol). Concentration of **Fc–cnq–1a** and **Fc–cnq–1b** is 3.0×10^{-4} M. Plots of logarithm of the absorbance as a function of the concentration of Be^{2+} for **Fc–cnq–1a** (c), for **Fc–cnq–1b** (d).

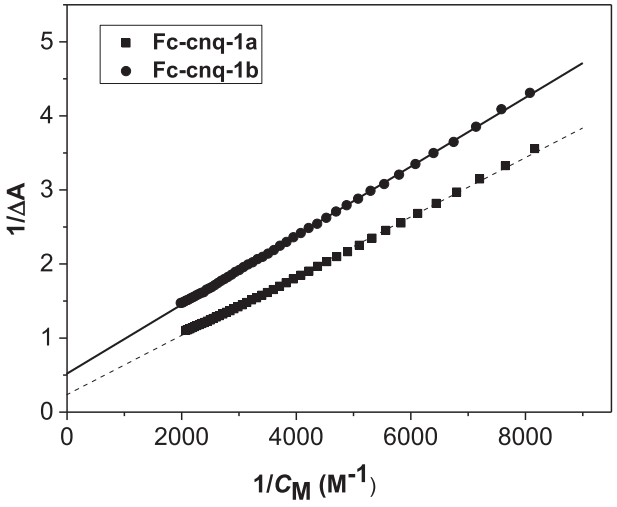


Fig. 12. Benesi-Hildebrand plots for the complexation reactions of the metal cation, Be^{+2}, with sensors **Fc–cnq–1a** and **Fc–cnq–1b**.

most competing metal ions such as alkali, alkaline earth and transition metal ions without using masking agent, and "naked eye" recognition of Be^{2+} ion in a significantly short response time.

The competitive experiments of sensors **Fc–cnq–1a** and **Fc–cnq–1b** with other metal ions in the presence of Be^{2+} ion were performed to understand the influence of the other metal ions on Be^{2+} ion binding (see Fig. 13). These experiments revealed that the change in the absorbance caused by Be^{2+} ion mixed with the other metal ions was almost similar to that caused by Be^{2+} ion alone, indicating none of the tested metal ions interfered with the binding of sensors **Fc–cnq–1a** and **Fc–cnq–1b** with Be^{2+}.

A potential mechanism of the binding of **Fc-cnq-1a/1b** towards Be^{2+} was proposed that the binding between the sensors having a convenient crown ether receptor (benzo-9-crown-3) with a right size (about 0.26 Å) on naphthoquinone core as chelating site and Be^{2+} ion take places via the ion dipol interaction. When Be^{2+} ion binds to oxygen donor atoms on macrocyclic crown ether ring, the electron donating ability of the macrocyclic decreases and result in an increasing electron acceptor character of naphthoquinone. This result probably favors permanently oxidation of ferrocene unit in the molecule depending on temperatures, thereby blocking the intramolecular charge-transfer (ICT) transition between the ferrocenyl donor and naphthoquinonyl acceptor center as observed in the experiments.

3.3. Theoretical calculations

In this study, the electro-optical properties of the compounds of **Fc–cnq–1a**, **Fc–cnq–1b** and their Be^{+2} complexes were calculated with DFT. In both **Fc–cnq–1a** and **Fc–cnq–1b**, vertical excitation energies with single excitations were performed with TDDFT calculations. The molecular orbitals, estimated by Koopman's theorem, are sketched for **Fc–cnq–1a** and **Fc–cnq–1b** in Fig. 14 and Fig. S20, respectively.

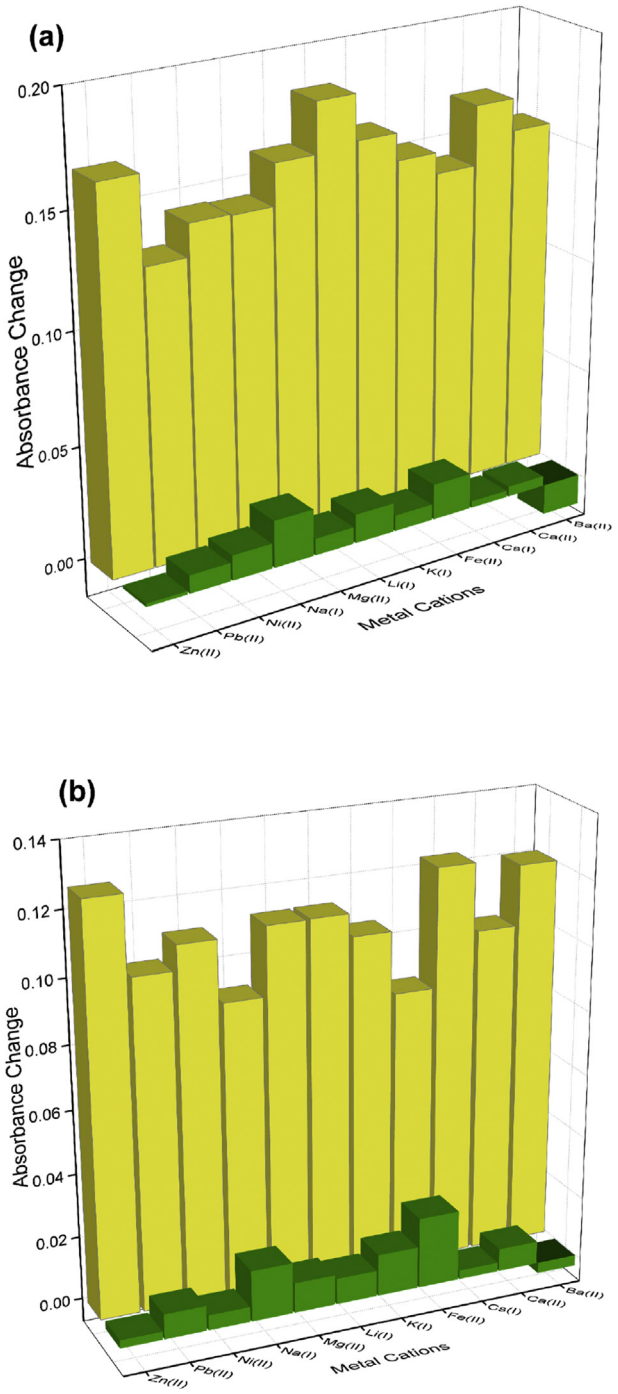


Fig. 13. Results of the competition experiments between Be^{2+} and selected metal ions (green column: competing ions, yellow column: competing ions + Be^{2+} ion). (a) for **Fc–cnq–1a** and (b) **Fc–cnq–1b**. Concentration of **Fc–cnq–1a** and **Fc–cnq–1b** is 1.7×10^{-4} M. (For interpretation of the references to color in this figure legend, the reader is referred to the Web version of this article.)

As seen Fig. 14 and Fig. S20, the minimum energy geometries and molecular orbital patterns are almost similar for **Fc–cnq–1a** and **Fc–cnq–1b**. In **Fc–cnq–1a**, the orientation of the crown ether oxygens allows their lone pairs to contribute to the delocalized napthoquinone system. This is reflected in the shortened C-O_{ether} bond length (1.36 Å and 1.38 Å) with respect to typical C-O bond length and the HOMO-4, HOMO-3, LUMO+1 and LUMO+2 molecular orbital schemes that act in n,π-π* transitions. HOMO, HOMO-1 and HOMO-2 mainly localize on the ferrocenyl moiety whereas HOMO-3 and HOMO-4 have contribution almost from the whole system. LUMO and LUMO+1 are mainly comprised of the napthoquinone moiety. The HOMO-LUMO transition, calculated as 0.77 eV, exhibits a well-defined charge transfer transition. The band gap approximated as the difference in HOMO-LUMO energies is lower than the electrochemical data (1.28 eV), which may be due to the level of theory or due to transitions being calculated on the ground state geometry. However, the data is good enough to get a qualitative picture of the systems.

A band at 675.57 nm, solely formed from HOMO-3 to LUMO with a moderate oscillator strength, (f = 0.0157) depicts a charge transfer transition in line with the experimental transition seen at 670 nm (Table 1). The biggest oscillator strength belonged to a transition of 350.53 nm (f = 0.2830) in calculations which mostly comprised of HOMO-3 to LUMO+1 absorption and indicated a π-π* transition. This result is in harmony with the UV spectrum, where one of the most intense transitions is seen at 333 nm. **Fc–cnq–1b** shows almost the same geometric and electro-optical features. The calculated band gap as approximated from Koopman is 0.84 ev. In **Fc–cnq–1b**, HOMO energy value decreased (−0.16363 au in **Fc–cnq–1a** vs −0.16568 au in **Fc–cnq–1b**) and the LUMO is increased (−0.13536 au in **Fc–cnq–1a** vs −0.13495 au in **Fc–cnq–1b**) with respect to its linear analogue. This is in line with the experimental red shift observed for **Fc–cnq–1a** where the HOMO-LUMO difference is lower. The experimental distinctive CT band at 649 nm has appeared at 622.64 nm in TD-DFT calculations for **Fc–cnq–1b** which is due to HOMO-3 to LUMO absorption. The calculated highest oscillator strength is at 341.11 nm which involve HOMO-4 to LUMO+1 transition, with n,π-π* transition.

It is known from the literature that small crown ethers and azacycles can bind to small metal cations due to their ionophoric ability [47–51]. The Be^{+2} complexed **Fc–cnq–1a** and **Fc–cnq–1b** are presented in Fig. 15.

Be^{+2} ion binds to etheric oxygens like a scorpionate ligand. This binding disturbs the contribution of oxygen atoms to delocalization of the napthoquinone system and increases the C-O bond to ca 1.43 Å in both **Fc–cnq–1a** and **Fc–cnq–1b**. Be^{2+} binds almost symmetrically to ether oxygens (at 1.62–1.63 Å) in **Fc–cnq–1a** and **Fc–cnq–1b**. As in uncomplexed structures, the HOMOs of Be^{2+} complexed **Fc–cnq–1a** and **Fc–cnq–1b** are mainly concentrated on ferrocenyl units and LUMOs on napthoquinone moiety (Fig. 15).

4. Conclusions

In summary, we have designed, synthesized, and characterized new organometallic ferrocene–quinone–crown ether triad molecules **Fc–cnq–1a** and **Fc–cnq–1b** as the first example of probes for selective and sensitive sensing trace amount of Be^{2+} ion among Li^+, Na^+, K^+, Cs^+, Mg^{2+}, Ca^{2+}, Ba^{2+}, Fe^{2+}, Ni^{2+}, Zn^{2+}, and Pb^{2+} cations.

The sensors show colorimetric and “naked eye” recognition of Be^{2+} ion, which could be practically monitored by gradually diminishing the intramolecular charge-transfer (CT) transition between the ferrocenyl donor and naphthoquinonyl acceptor center [e_π (HOMO–Fc) → e_{π^*} (LUMO–cnq)]. The following important properties of the new sensors can be summarized as conclusion: The response times of the sensors are temperature dependent as expected and faster response times were obtained at 60 °C where the response times were measured as 2 min and 4 min for **Fc–cnq–1a** and **Fc–cnq–1b**, respectively. Very low detection limits, which is in the range of micro molar concentration levels of the Be^{+2} cation (5.41 μM), could be achieved. Finally, the selectivity of the sensors is very high and the sensors can selectively detect the Be^{+2} ion among the other metal ions without interference by using spectrophotometric titration technique. It could be mentioned for the real-life practical application of these proposed selective and

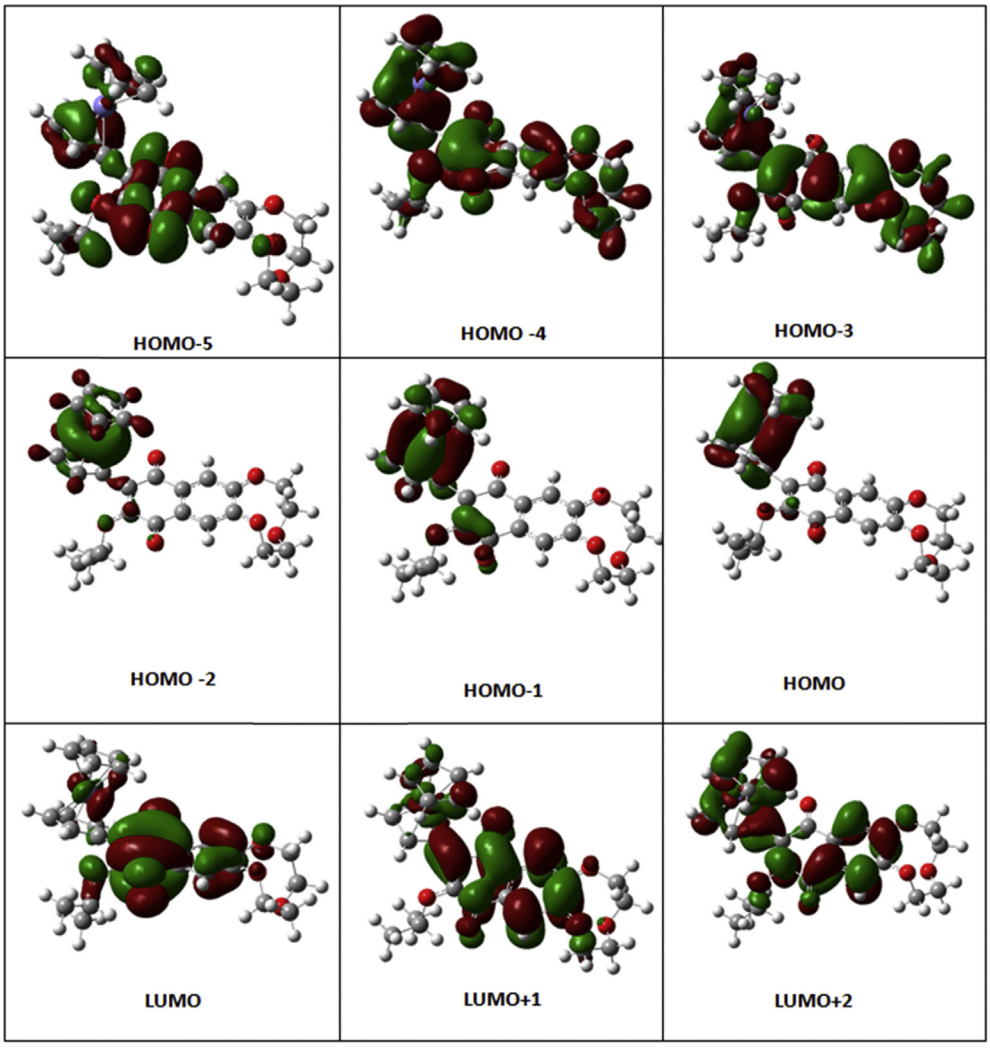


Fig. 14. Molecular Orbitals calculated at TD-B97D/TZVP//mPWPW91/6-31 + G(2d,2p) level for **Fc–cnq–1a** in DMF.

Table 1
Calculations on vertical electronic transitions of **Fc–cnq–1a** performed at TD-B97D/TZVP//mPWPW91/6-31 + G(2d,2p) level in DMF. Transitions with oscillator strength (f) bigger than 0.015 are presented. Please refer to Table S1 for the data of **Fc–cnq–1b**.

Energy for Transition (in eV)	Wavelength for the transition	Oscillator Strength	Major Contribution to Transition	
1.0646	1164.6	0.0499	HOMO-2→LUMO	HOMO-1→LUMO
1.8353	675.57	0.0157	HOMO-3→LUMO	
2.3091	536.95	0.0334	HOMO-4→LUMO	
2.4331	509.57	0.0287	HOMO-1→LUMO+1	
2.535	489.09	0.0104	HOMO-2→LUMO+1	
2.5709	482.26	0.0102	HOMO-7→LUMO	
2.7551	450.02	0.0455	HOMO-8→LUMO	
2.8999	427.54	0.038	HOMO-9→LUMO	
3.1134	398.23	0.0284	HOMO-11→LUMO	HOMO-10→LUMO
3.2994	375.77	0.0154	HOMO-1→LUMO+4	HOMO→LUMO+3
3.3462	370.53	0.0216	HOMO-12→LUMO	
3.4477	359.62	0.0662	HOMO-13→LUMO	HOMO-3→LUMO+1
3.4929	354.96	0.0505	HOMO-2→LUMO+4	
3.537	350.53	0.283	HOMO-3→LUMO+1	HOMO-2→LUMO+4
3.7614	329.63	0.0515	HOMO-4→LUMO+1	
3.9211	316.2	0.0422	HOMO-3→LUMO+2	
3.9597	313.12	0.0559	HOMO-14→LUMO	
4.1913	295.81	0.0422	HOMO-4→LUMO+2	
4.5402	273.08	0.0159	HOMO-3→LUMO+4	HOMO-2→LUMO+5
4.5522	272.36	0.0735	HOMO-3→LUMO+4	
4.6818	264.82	0.0179	HOMO-11→LUMO+1	
4.7103	263.22	0.092	HOMO-10→LUMO+1	HOMO-8→LUMO+2
4.7422	261.45	0.0413	HOMO-4→LUMO+4	
4.8028	258.15	0.0311	HOMO-5→LUMO+4	HOMO-7→LUMO+3
4.8248	256.97	0.019	HOMO-5→LUMO+4	

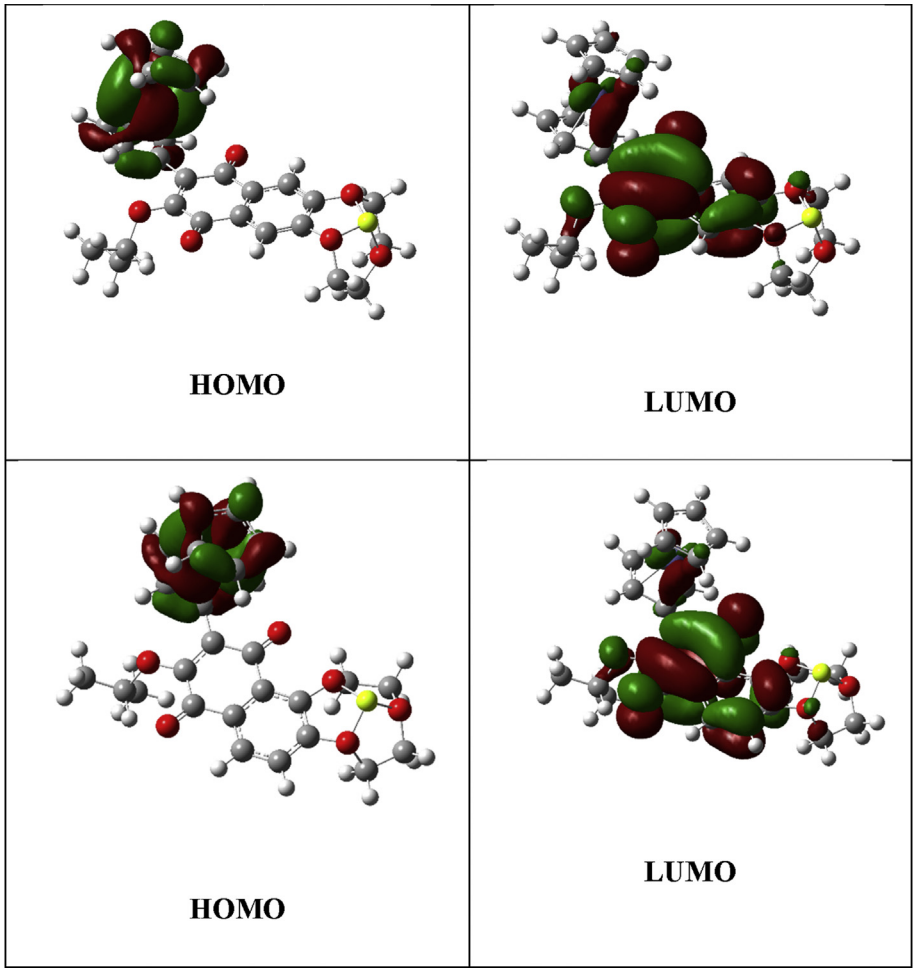


Fig. 15. HOMO and LUMO Molecular Orbitals of Be^{+2} complexed **Fc–cnq–1a** (1st row) and **Fc–cnq–1b** (2nd row) calculated at TD-B97D/TZVP//mPWPW91/6-31 + G(2d,2p) level in DMF.

sensitive chemosensors that are able to monitor the concentration of Be^{2+} ion without interference in water supplies and atmosphere contaminated by beryllium via discharges from anthropogenic sources.

In addition to the experiments, the electro-optical properties of **Fc–cnq–1a**, **Fc–cnq–1b** their Be^{+2} complexes have also been calculated by quantum mechanical calculations in order to elucidate their geometries and the molecular orbitals.

Acknowledgments

This work was supported by The Scientific and Technical Research Council of Turkey (TUBİTAK, Project no: 113Z309).

Appendix A. Supplementary data

Supplementary data related to this article can be found at https://doi.org/10.1016/j.jorganchem.2018.05.004.

References

[1] Z. Fabiola, A. Caballero, E. Arturo, A. Tarraga, P. Molina, Org. Lett. 10 (2008) 41–44.
[2] Z. Fabiola, A. Caballero, E. Arturo, A. Tarraga, P. Molina, J. Org. Chem. 74 (2009) 4787–4796.
[3] H. Xue, X.J. Tang, L.Z. Wu, L.P. Zhang, C.H. Tung, J. Org. Chem. 70 (2005) 9727–9734.
[4] D. Remeter, P. Blanchard, M. Allain, I. Grosu, J. Roncali, J. Org. Chem. 72 (2007) 5285–5290.
[5] M. Alfonso, A. Tárraga, P. Molina, Inorg. Chem. 52 (2013) 7487–7496.
[6] T. Romero, A. Caballero, A. Espinosa, A. Tárraga, P. Molina, Dalton Trans. (2009) 2121–2129.
[7] A. Thakur, D. Mandal, S. Ghosh, Anal. Chem. 85 (2013) 1665–1674.
[8] R. Pandey, R.K. Gupta, M. Shahid, B. Maiti, A. Misra, D.S. Pandey, Inorg. Chem. 51 (2012) 298–311.
[9] H. OuYang, Y. Gao, Y.A. Yuan, Tetrahedron Lett. 54 (2013) 2964–2966.
[10] A.S. Amin, Anal. Chim. Acta 437 (2001) 265–272.
[11] K. Ashley, A. Agrawal, J. Cronin, J. Tonazzi, T.M. McCleskey, A.K. Burrell, D.S. Ehler, Anal. Chim. Acta 584 (2007) 281–286.
[12] A. Afkhami, T. Madrakian, E. Bozorgzadeh, M. Bahram, Talanta 71 (2007) 1103–1109.
[13] X. Ji, W. Shi, S. Zhang, M. Wei, D.G. Evans, X. Duan, Anal. Chim. Acta 728 (2012) 77–85.
[14] H.B. Singh, N.K. Agnihotri, V.G. Singh, Talanta 47 (1998) 1287–1296.
[15] M.R. Ganjali, M. Ghorbani, P. Norouzi, A. Daftari, M. Faal-Rastegar, A. Moghimi, Sensor. Actuator. B Chem. 100 (2004) 315–319.
[16] C.Y. Wong, J.D. Woollins, Coord. Chem. Rev. 130 (1994) 243–273.
[17] K.A. Walsh, Beryllium Chemistry and Processing, first ed., ASM International, USA, 2009.
[18] R.C. Rapp, Encyclopedia of the Alkaline Earth Compounds, Elsevier, Oxford, UK, 2013.
[19] E.C. McCanlies, K. Kreiss, M. Andrew, A. Weston, Am. J. Epidemiol. 157 (2003) 388–398.
[20] J.D. Stoeckle, H.L. Hardy, A.L. Weber, Am. J. Med. 46 (1969) 545–561.
[21] R.T. Sawyer, B.J. Day, V.A. Fadok, M. Chiarappa-Zucca, L.A. Maier, A.P. Fontenot, L. Silveira, L.S. Newman, Am. J. Respir. Cell Mol. Biol. 31 (2004) 470–477.
[22] A.L. Reeves, D. Deitch, A.J. Vorwald, I. Cancer Res 27 (1967) 439–445.
[23] K.C. Meyer, Beryllium and lung disease, Chest 106 (1994) 942–946.
[24] USEPA, Technology Transfer Network, Beryllium and Compounds. Office of Air Quality Planning and Standards, United States Environmental Protection Agency, Research Triangle Park (NC), 1998.
[25] I.A.R.C. Beryllium, Cadmium, Mercury, and Exposures in the Glass Manufacturing Industry. IARC Monographs on the Evaluation of Carcinogenic Risks to Humans, International Agency for Research on Cancer, Lyon (France), 1993.
[26] WHO, Beryllium and Beryllium Compounds. Concise International Chemical Assessment Document No. 32, World Health Organization, Geneva, 2001.
[27] E.B. Sandell, H. Hnishi, Photometric Determination of Trace Metals. Part 3, Wiley, New York, 1978.
[28] Y.Y. Vin, S.M. Khopkar, Analyst 113 (1988) 175–177.
[29] H.B. Singh, N.K. Agnihotri, V.K. Singh, Talanta 47 (1998) 1287–1296.
[30] F.D. Snell, C.L. Hilton, Encyclopedia of Industrial Chemical Analysis, vol. 7, John Wiley, New York, 1968, pp. 112–115.
[31] M.J. Shaw, S.J. Hill, P. Jones, P.N. Nesterenko, J. Chromatogr. A 876 (2000) 127–133.
[32] H. Matsumiya, H. Hoshino, Anal. Chem. 75 (2003) 413–419.
[33] W. Bashir, B. Paull, J. Chromatogr. A 910 (2001) 301–309.
[34] F.D. Snell, Beryllium, in: Photometric and Fluorometric Methods of Analysis Metals, Part 1, Wiley, New York, 1978, pp. 661–701.
[35] C.I. Measures, J.M. Edmond, Anal. Chem. 58 (1986) 2065–2069.
[36] J.L. Burguera, M. Burguera, C. Rondon, P. Carrero, M.R. Brunetto, Y. Petit de Pena, Talanta 52 (2000) 27–37.
[37] P. Štěpnička, in: Ferrocenes: Ligands, Materials and Biomolecules, John Wiley &Sons Ltd, Chichester, 2008.
[38] D.R. van Staveren, N. Metzler-Nolte, Chem. Rev. 104 (2004) 5931–5985.
[39] G. Tollin, in: V. Balzani (Ed.), Electron Transfer in Chemistry, vol 4, Wiley-VCH, Weinheim, 2001, p. 202.
[40] C. Costentin, Chem. Rev. 108 (2008) 2145–2179.
[41] A.J. Swallow, in: B.L. Trumpover (Ed.), Function of Quinones in Energy Conserving Systems, Academic Press, New York, 1982. Chapter 3.
[42] J.Q. Chambers, in: Z. Patai (Ed.), The Chemistry of the Quinonoid Compounds; Rappoport, vol. II, J. Wiley&Sons, New York, 1988, p. 719. Chapter 12.
[43] E.E. Langdon-Jones, S.J.A. Pope, Coord. Chem. Rev. 269 (2014) 32–53.
[44] S. Devaraj, D. Saravanakumar, M. Kandaswamy, Tetrahedron Lett. 48 (2007) 3077–3081.
[45] P.D. Beer, P.A. Gale, G.Z. Chen, Coord. Chem. Rev. (1999) 185–186, 3–36.
[46] P.L. Boulas, M. Gómez-Kaifer, L. Echegoyen, Angew. Chem. Int. Ed. 37 (1998) 216–247.
[47] C.J. Pedersen, J. Am. Chem. Soc. 92 (1970) 391–394.
[48] C.J. Pedersen, J. Am. Chem. Soc. 92 (1970) 386–391.
[49] C.J. Pedersen, J. Am. Chem. Soc. 89 (1967) 2495–2496.
[50] R.M. Izatt, K. Pawlak, J.S. Bradshaw, R.L. Bruening, Chem. Rev. 95 (1995) 2529–2586.
[51] B. Fabre, J. Simonet, Coord. Chem. Rev. (1998) 178–180, 1211–1250.
[52] B. Valeur, I. Leray, Coord. Chem. Rev. 205 (2000) 3–40.
[53] P.D. Beer, E.J. Hayes, Coord. Chem. Rev. 240 (2003) 167–189.
[54] B. Yucel, B. Sanli, H. Soylemez, I. Yilmaz, Tetrahedron 67 (2011) 1406–1421.
[55] M. Zora, B. Yucel, S. Acikalin, Tetrahedron Lett. 44 (2003) 2237–2241.
[56] K.S. Chan, H. Zhang, Synth. Commun. 25 (1995) 635–639.
[57] P.D. Beer, in: A.G. Sykes (Ed.), Adv. Inorg. Chem. Rad, vol 39, Academic Press, 1992, pp. 79–157.
[58] P.D. Beer, Chem. Soc. Rev. 18 (1989) 409–450.
[59] M.C. Grossel, D.G. Hamilton, J.I. Fuller, E. Millan-Barrios, J. Chem. Soc., Dalton Trans. (1997) 3471–3477.
[60] M.J.L. Tendero, A. Benito, R. Martinez-Manez, J. Soto, J. Paya, A.J. Edwards, P.R. Raithby, J. Chem. Soc., Dalton Trans. (1996) 343–351.
[61] H. Zhang, B. Zhou, H. Li, D.H. Qu, H. Tian, J. Org. Chem. 78 (2013) 2091–2098.
[62] M.A. Rahman, N.H. Kwon, M.S. Won, M.H. Hyun, Y.B. Shim, Anal. Chem. 76 (2004) 3660–3665.
[63] R.E. Wolf, S.R. Cooper, J. Am. Chem. Soc. 106 (1984) 4646–4647.
[64] K. Sugihara, H. Kamiya, M. Yamaguchi, T. Kaneda, S. Misumi, Tetrahedron Lett. 22 (1981) 1619–1622.
[65] H. Bock, B. Hierholzer, F. Vögtle, G. Hollmann, Angew Chem. Int. Ed. Engl. 23 (1984) 57–58.
[66] M. Delgado, R.E. Wolf Jr., J.R. Hartman, G. McCafferty, R. Yagbasan, S.C. Rawle, D.J. Watkin, S.R. Cooper, J. Am. Chem. Soc. 114 (1992) 8983–8991.
[67] A.A. Aguilar, E.P. Cabrera, L.S. Liebeskind, Arkivoc (2004) 156–162.
[68] G.W. Buchanan, A.B. Driega, A. Moghimi, C. Bensimon, K. Bourque, Can. J. Chem. 71 (1993) 951–959.
[69] M. Dagdevren, I. Yilmaz, B. Yucel, M. Emirik, J. Phys. Chem. B 119 (2015) 12464–12479.
[70] S.B. Colbran, S.T. Lee, D.G. Lonnon, F.J.D. Maharaj, A.M. McDonagh, K.A. Walker, R.D. Young, Organometallics 25 (2006) 2216–2224.
[71] S. Barlow, H.E. Bunting, C. Ringham, J.C. Green, G.U. Bublitz, S.G. Boxer, J.W. Perry, S.R. Marder, J. Am. Chem. Soc. 121 (1999) 3715–3723.
[72] S. Barlow, D. O'Hare, Chem. Rev. 97 (1997) 637–670.
[73] E. Gebert, A.H. Reis, J.S. Miller, H. Rommelmann, A.J. Epstein, J. Am. Chem. Soc. 104 (1982) 4403–4410.
[74] I. Yilmaz, New J. Chem. 32 (2008) 37–46.
[75] I. Yilmaz, S. Arslan, S. Guney, I. Becerik, Electrochim. Acta 52 (2007) 6611–6621.
[76] K.M. Kadish, T. Nakanishi, A. Gürek, V. Ahsen, I. Yilmaz, J. Phys. Chem. B 105 (2001) 9817–9821.
[77] T. Nakanishi, I. Yilmaz, N. Nakashima, K.M. Kadish, J. Phys. Chem. B 107 (2003) 12789–12796.
[78] I. Yilmaz, T. Nakanishi, A. Gurek, K.M. Kadish, J. Porhyr. Phthalocya 7 (2003) 227–238.
[79] R. Chang, Physical Chemistry for the Biosciences, University Science Books, Sausalito (CA), 2005, pp. 311–347.
[80] H.A. Benesi, J.H. Hildebrand, J. Am. Chem. Soc. 71 (1949) 2703–2707.
[81] S. Bhattacharya, S.C. Bhattacharya, M. Banerjee, J. Phys. Chem. A 108 (2004) 10783–10788.
[82] S. Mitra, R. Das, S. Mukherjee, J. Phys. Chem. B 102 (1998) 3730–3735.
[83] A. Ajayaghosh, P. Carol, S. Sreejith, J. Am. Chem. Soc. 127 (2005), 14962–1963.